ORIGINAL ARTICLE

Breaking Limits of Li-Ion Batteries with High-Voltage Spinel LiNi$_{0.5}$Mn$_{1.5}$O$_4$ Nanofiber/Carbon Nanotube Composite Cathodes

Na-Yeong Kim[1] · Min Kyoung Gi[1] · Zubair Ahmed Chandio[2] · Jeong-Ho Park[1] · Jun Young Cheong[2] · Ji-Won Jung[1]

Abstract

Spinel-structured LiNi$_{0.5}$Mn$_{1.5}$O$_4$ (LNMO), which is used as a cathode material for lithium-ion batteries, offers economic and eco-friendly advantages, as it operates at a high voltage of 5 V and does not require expensive cobalt. However, challenges such as low electronic conductivity and volume changes due to phase transitions during charging and discharging at 3 V or lower persist, resulting in capacity degradation. In this study, LNMO nanofibers were created using the electrospinning method to tackle the volume expansion issue and maintain structural integrity of the material. In addition, the electrode was constructed with carbon nanotubes as a conductive material to improve electronic conductivity. Electrochemical evaluations showed that LNMO nanofibers combined with carbon nanotubes exhibited a higher capacity and outstanding cyclability compared to LNMO powder.

Keywords LiNi$_{0.5}$Mn$_{1.5}$O$_4$ · Nanofibers · Carbon nanotubes · Electrospinning · Li-ion batteries

Introduction

Lithium-ion batteries offer numerous advantages over other types of metal-ion batteries, such as a high energy density, high operating voltage, and low discharge rate [1–3]. They have found widespread use in various applications, including electric vehicles and hybrid electric vehicles, where a higher energy density is essential to increase driving range [4–6]. A battery comprises four essential components: an anode, cathode, separator, and electrolyte. However, the cathode materials play a crucial role in determining the battery's capacity, depending on how much lithium they contain and how effectively they function at high voltage [7]. Therefore, the development of efficient cathode materials is vital in improving the performance of lithium-ion batteries.

Among the appealing cathode materials, LiNi$_{0.5}$Mn$_{1.5}$O$_4$ (LNMO), with its spinel structure, has gained significant attention as an economical and eco-friendly option. This is due to its high operating voltage (4.7 V vs. Li/Li$^+$) achieved through the Ni^{2+}/Ni^{4+} redox reaction, and the absence of expensive and scarce cobalt (Co) [8–11]. However, electrolyte decomposition occurs at high or low voltage (< 3.0 V vs. Li/Li$^+$), and the reaction with the electrode is chemically unstable [12, 13]. As a result, researchers aim to discharge the material at 3 V or less to enhance its capacity. Moreover, there are challenges such as reduced capacity over cycles due to volume changes from a cubic to a tetragonal structure during charging and discharging, as well as limited rate capability resulting from low electronic and ionic conductivity.

To solve these problems of LNMO, nanostructuring of LNMO is being actively researched [14, 15]. In particular, it is known that nano-sized materials can solve volume changes and capacity degradation due to phase transitions.

✉ Jun Young Cheong
Jun.Cheong@uni-bayreuth.de

✉ Ji-Won Jung
jwjung4@ulsan.ac.kr

Na-Yeong Kim
kny0103013@gmail.com

Min Kyoung Gi
rlalsrud99@gmail.com

Jeong-Ho Park
fjdk9936@naver.com

[1] School of Materials Science and Engineering, University of Ulsan, Ulsan 448776, Korea

[2] Department of Chemistry and Bavarian Center for Battery Technology (BayBatt), University of Bayreuth, Universitätsstraße 30, 95447 Bayreuth, Germany

This is because the large specific surface area allows for a wide interfacial reaction with the electrolyte, and the short lithium-ion diffusion length allows for a fast kinetic reaction. In recent years, S. Tao has developed a straightforward method to synthesize composites consisting of nanoscale TiO_2-coated LNMO, which exhibit outstanding rate capability and excellent cycling ability [16]. Zhao et al. have developed nanorod materials and found that they have excellent cycling capability and improved capacity retention [17]. Although the nanoengineering of LNMO is important, there are still problems such as low electronic conductivity and limitations in the rational design of LNMO and composite with electrically conductive materials [18].

In this study, one-dimensional (1D) nanofiber-like LNMOs were fabricated using a simple electrospinning method—a versatile, cost-effective, and functional technique for producing 1D nanofibers—followed by heat treatment. By creating 1D nanofibers consisting of interconnected polycrystalline LNMO nanoparticles, the ionic conductivity could potentially be enhanced through interfacial reactions facilitated by shorter ionic diffusion lengths and larger specific surface areas. This would allow the LNMO nanofibers to operate stably at low potentials (up to 2.0 V during discharging) without phase transformation. Moreover, to address the low electronic conductivity of LNMO, carbon nanotubes with high electrical conductivity were incorporated to fabricate electrodes. According to a first cycle test at 1C, the LNMO nanofiber electrode, coated with carbon nanotubes, exhibited a capacity of 134 mAh g^{-1}, which was 48 mAh g^{-1} higher than that of the LNMO powder electrode.

Experimental

Synthesis of LNMO Nanofibers and Powders

The LNMO nanofibers were prepared by electrospinning and subsequent heat treatment. Initially, an appropriate amount of mixed $LiC_2H_3O_2 \cdot 2H_2O$ ($\geq 63\%$, Sigma-Aldrich), $Ni(C_2H_3O_2) \cdot 4H_2O$ (98%, Sigma-Aldrich), and $Mn(C_2H_3O)_2 \cdot 4H_2O$ (99.0%, Sigma-Aldrich) in a molar ratio of 1.1:0.5:1.5 was dissolved in 5 ml of *N,N*-dimethylformamide (DMF, 99.8%, Sigma-Aldrich) and stirred at room temperature for 4 h. Subsequently, 0.5 g of polyacrylonitrile (Mw: 150,000 g/mol, Sigma-Aldrich) was added to the solution and stirred at 80 °C for 12 h. The precursor solution was loaded into a plastic syringe with a 23-gauge tip needle. The voltage was 11–13 kV, and the solution feeding rate was controlled at 14 µl/min, and aluminum foil was used to collect the nanofibers. The as-spun fibers were heated at 800 °C for 5 h with a heating rate of 5 °C/min under air atmosphere to obtain LNMO oxide nanofibers. As a reference sample, LNMO powders were synthesized by the conventional solid-state reaction method. The Li_2CO_3 ($\geq 99.0\%$, Sigma-Aldrich) NiO (99.8%, Sigma-Aldrich), and $Mn(C_2H_3O_2)_2 \cdot 4H_2O$ ($\geq 99.0\%$, Sigma-Aldrich) precursors were homogeneously mixed and then thoroughly ground for 30 min. The mixed powder is exposed to the calcination temperature of 850 °C for 12 h and 600 °C for 6 h with a heating rate of 5 °C min^{-1} under air surroundings in an alumina crucible.

Materials Characterizations

The morphology of LNMO nanofibers and powders was observed by scanning electron microscope (SEM; UHR FE-SEM (SU8230) by Hitachi High-Technologies Corp., Japan). TEM and HR-TEM images were taken by JEOL Cs-corrected scanning transmission electron microscope. The crystal structure of the nanofibers was characterized using X-ray diffraction (XRD; MiniFlex600, Rigaku) at a scan rate of 10° min^{-1}. To determine the oxidation state of the manufactured LNMO nanofibers, X-ray photoelectron spectroscopy (XPS; K-alpha +, Thermo Scientific) analysis was also performed.

Preparation of LNMO/CNT Composites and Electrochemical Evaluation

LNMO/CNT cathodes were prepared by mixing 75 wt% active material, 5 wt% CNT and 10 wt% super-P and 10 wt% polyvinylidene fluoride (PVDF) in N-methyl-2-pyrrolidone (NMP). The LNMO powder, serving as the active material, along with super-P and PVDF, was blended in a weight ratio of 80:10:10 in NMP. CNT content in the composite cathode material is reported to be optimum for electrochemical performance at 5 wt% content of total amount of the composite to be used as a cathode material for lithium-ion batteries. Wu et al., prepared polyimide/CNT nanocomposite, with CNT content from 1 to 10 wt%, as a cathode material for lithium-ion batteries and reported that the sample with 5% CNT content showed a better electrochemical performance compared to other samples from 1 to 10 wt% CNT content loading in the composite [19]. Similarly, Cui et al., studied the electrochemical performance of $VOSO_4$@CNT composite material as a cathode for lithium-ion battery and demonstrated a good performance of the composite material at 5 wt% CNT content loading [20]. The slurry was pasted casting onto aluminum foil with a manual doctor blade. This cathode electrode was dried for 40 min at 100 °C followed by pressing at 70 MPa, with a final drying process being conducted under vacuum at 120 °C for 6 h. The loading mass of active materials was 2.2–2.4 mg/cm^2. Electrochemical performance was tested via half-cell CR2032 coin type cells. Celgard 2400 was used as a separator and 1.2 M $LiPF_6$ in EC: EMC = 3:7(v/v) + VC 2 wt% was used as electrolyte.

The cells were assembled in an Ar-filled glove box. The electrochemical measurements of the cells were performed by a cycler (WonaTech) battery-testing system at 30 °C.

Results and Discussion

Fabrication of LNMO Nanofibers and LNMO/CNT Composites

One-dimensional nanostructured LNMO nanofibers were synthesized by using conventional electrospinning method (see details in the experimental section) (Fig. 1). Three different elements such as Li, Ni and Mn were contained in the electrospinning solution using every single element precursor (first step). After appropriate stirring, the solution was transferred to the electrospinning apparatus and electrospun by applying high voltage over 15 kV. As-spun nanofiber membranes were obtained (second step). Then, the as-spun nanofibers were thermally treated in a tube furnace in a pure O$_2$ atmosphere for LNMO to be a perfect crystalline, but not to be defective [21]. This third step produced the 1D LNMO nanofibers consisting of interconnected polycrystalline LNMO nanoparticles. To overcome the issue of intrinsically low electronic conductivity, the LNMO nanofibers were homogeneously mixed with multi-walled carbon nanotubes (MWCNTs) employing a mechanical mixer (final step). The composite product was used to fabricate cathode and evaluate lithium-ion battery performance.

Characterizations of Morphology and Chemical States

Figure 2a shows the scanning electron microscopy (SEM) image of the polyacrylonitrile (PAN)/acetate composite fiber in the as-spun state after electrospinning. The image
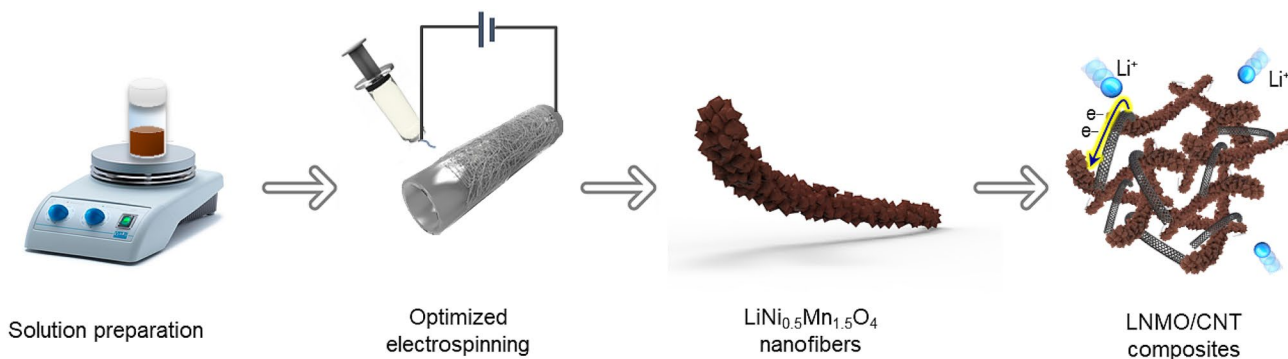

Fig. 1 Schematic of the LNMO/CNT composite preparation process. (1) Electrospinning solution preparation, (2) optimized electrospinning, (3) production of LNMO nanofibers, and (4) final mixing of LNMO and MWCNTs
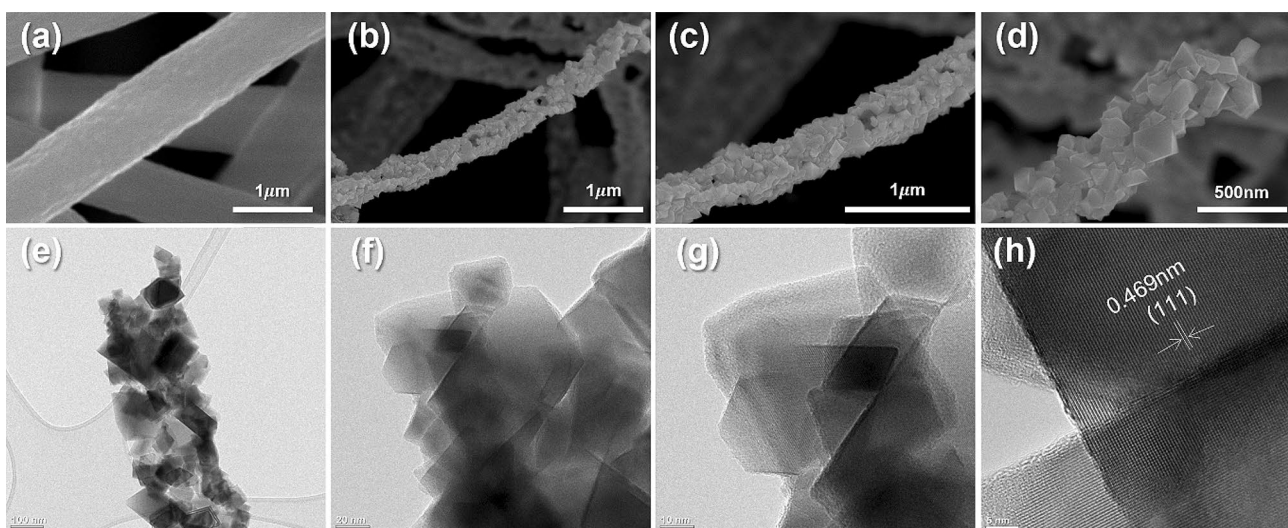

Fig. 2 **a** SEM images of as-spun PAN/acetate composite fiber **b–d** SEM image of LNMO nanofibers after calcination for 5 h 800 °C in air. **e–g** TEM image and **h** HR-TEM image of LNMO NFs after calcination for 5 h 800 ℃ in air

reveals that the electrospinning method results in uniform fibers with an average diameter of approximately 400 nm. So, upon heat treatment of the as-spun fibers at 800 °C for 5 h, the LNMO nanoparticles form one-dimensional fibers, as shown in Fig. 2b–d. Similarly, the studies involved in the preparation of crystalline nanofiber reported that a thermal treatment at 800 °C produced optimum [22]. Moreover, 800 °C was used as the reference temperature at which previous work employed for comparison between sample with and without sulfur substitution, which might be the suitable temperature for comparison [23]. The decrease in nanofiber size and surface roughness could be attributed to the depletion of polymer material within the nanofibers due to heat treatment. The nanoscale dimensions of the material are beneficial for lithium storage as the small particle size and reduced diffusion distance for lithium ions can enhance the performance of the material. This can result in improved efficiency and faster charging and discharging rates for lithium-ion batteries. In addition, the small pores between the nanoparticles can serve as void space to accommodate volume changes that occur during phase transitions upon (de) lithiation. We conducted a transmission electron microscopy (TEM) analysis to investigate the morphological and crystal structures (Fig. e–g). Our analysis confirmed that the LNMO nanoparticles were crystalline and interconnected, forming 1D nanofibers. The high-resolution TEM (HR-TEM) image

revealed that the as-synthesized LNMO nanofibers had a cubic crystal structure, as evidenced by the lattice fringe of (111) crystal planes with a lattice spacing of 0.469 nm (Fig. (h)). X-ray diffractometer (XRD) patterns further confirmed that both the LNMO nanofibers and LNMO powder possess $LiNi_{0.5}Mn_{1.5}O_4$ crystal structures with the Fd3m space group, where Ni and Mn ions are disordered in octahedral positions within a cubic spinel structure (JCPDS no. 80–2162; space group: Fd3m; $a = b = c = 8.170$) (Fig. 3a). The average crystallite sizes of the LNMO nanofibers and LNMO powders were calculated with Scherrer's equation from the XRD data. The average crystallite size of the LNMO powder was 52.55 nm, and the size of nanofiber crystalline treated at temperatures of 600 °C, 700 °C and 800 °C was 30.34 nm, 37.33 nm and 61.88 nm, respectively. The XRD data of the LNMO powders, which were prepared as a reference, matched well with that of the LNMO nanofibers (Fig. 3b). Although the starting phases of both the LNMO nanofibers and powders were cubic spinel, they can be transformed into tetragonal spinel if lithiated at a low voltage below 3.0 V_{Li} [12].

The possible phase transition between cubic and tetragonal structures is presented schematically in Fig. 3c. X-ray photoelectron spectroscopy (XPS) analysis was performed to analyze the surface of the material (Fig. 3d–f). Figure 3d shows the Mn 2p spectrum
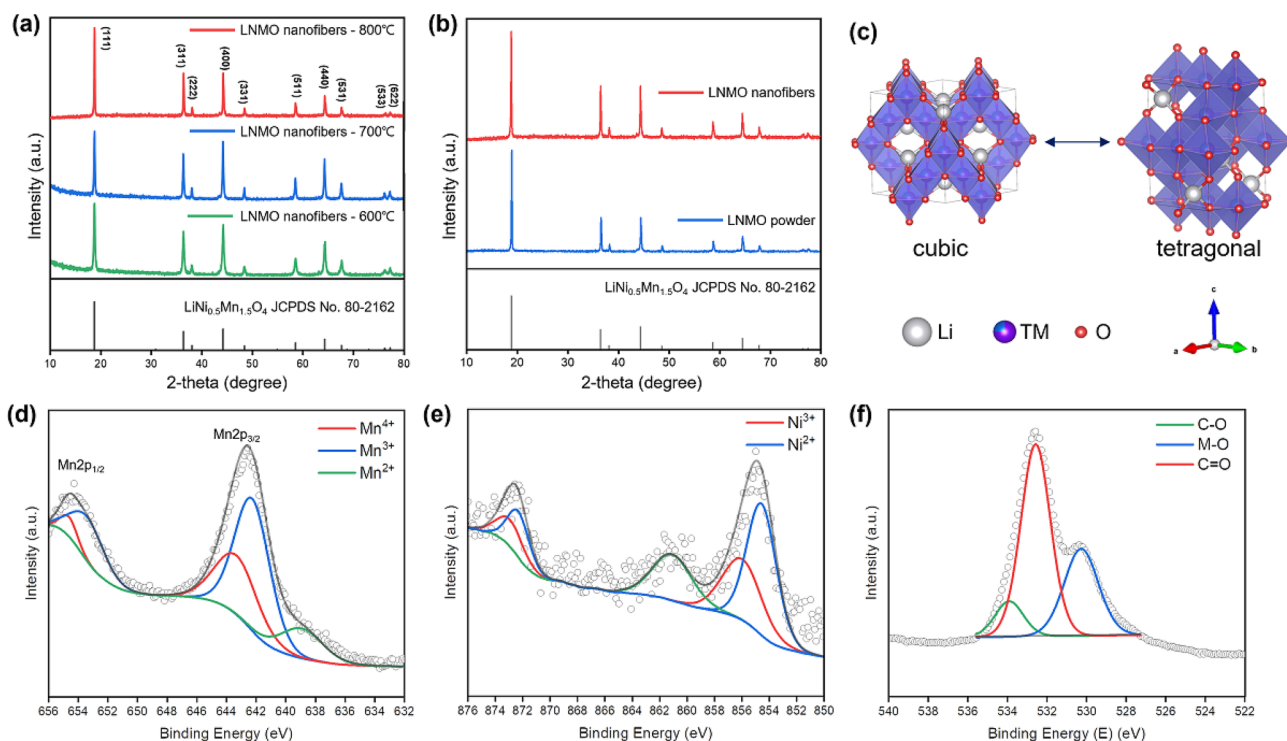

Fig. 3 XRD patterns of **a** the three LNMO nanofibers materials 600 °C, 700 °C, 800 °C and **b** the LNMO nanofibers and LNMO powder. **c** Schematic structures of disordered (Fd3m) and tetragonal (I41/amd) **d**–**f** XPS pattern of Mn 2p, Ni 2p and O 1s of LNMO NFs

of LNMO nanofibers, where double peaks of Mn $2p_{3/2}$ and Mn $2p_{1/2}$ were observed in the Mn $2p$ spectrum. It was found that the peak appearing at about 642.4 eV in Mn $2p_{3/2}$ represents the binding energy of Mn^{3+}, and the peak located at 643.7 eV represents the binding energy of Mn^{4+}. In addition, the O 1 s spectrum shows the binding of metal ions to oxygen at about 530.28 eV. The peaks registered at 532.58 and 533.88 eV within the O 1 s spectrum signify the presence of C–O and C = O functional groups [24]. The peak at 854.68 eV represents the binding energy of Ni^{2+}, and the peak at 856.2 eV represents the binding energy of Ni^{3+}, and the peak at 860.98 eV represents the binding energy of satellite spectrum [25]. These XPS results confirm that the LNMO nanofibers have transition metal elements with general oxidation states [26].

Electrochemical Performance of Li-Ion Battery Cells

Cycle voltammetry was conducted to analyze the electrochemical properties of the prepared LNMO nanofibers and LNMO powders, both at a scan rate of 0.1 mV/s. Figure 4a shows cyclic voltammetry for LNMO powders at a voltage range of 3.5–5 V, while Fig. 4b displays cyclic voltammetry for LNMO nanofibers at a voltage range of 2.0–4.8 V. Due to the nanostructuring effects of the LNMO nanofibers, the operating voltage can be lowered down to 2.0 V, which significantly expands the voltage window and offers advantages for achieving high energy density.

By introducing conductive CNTs, wide voltage windows and superior rate capabilities are expected. Both nanofiber and powder samples exhibited oxidation reactions of Ni^{2+}/ Ni^{3+} and Ni^{3+}/Ni^{4+}, indicated by the generated peaks at around 4.7 V during the initial charging cycle [27, 28].
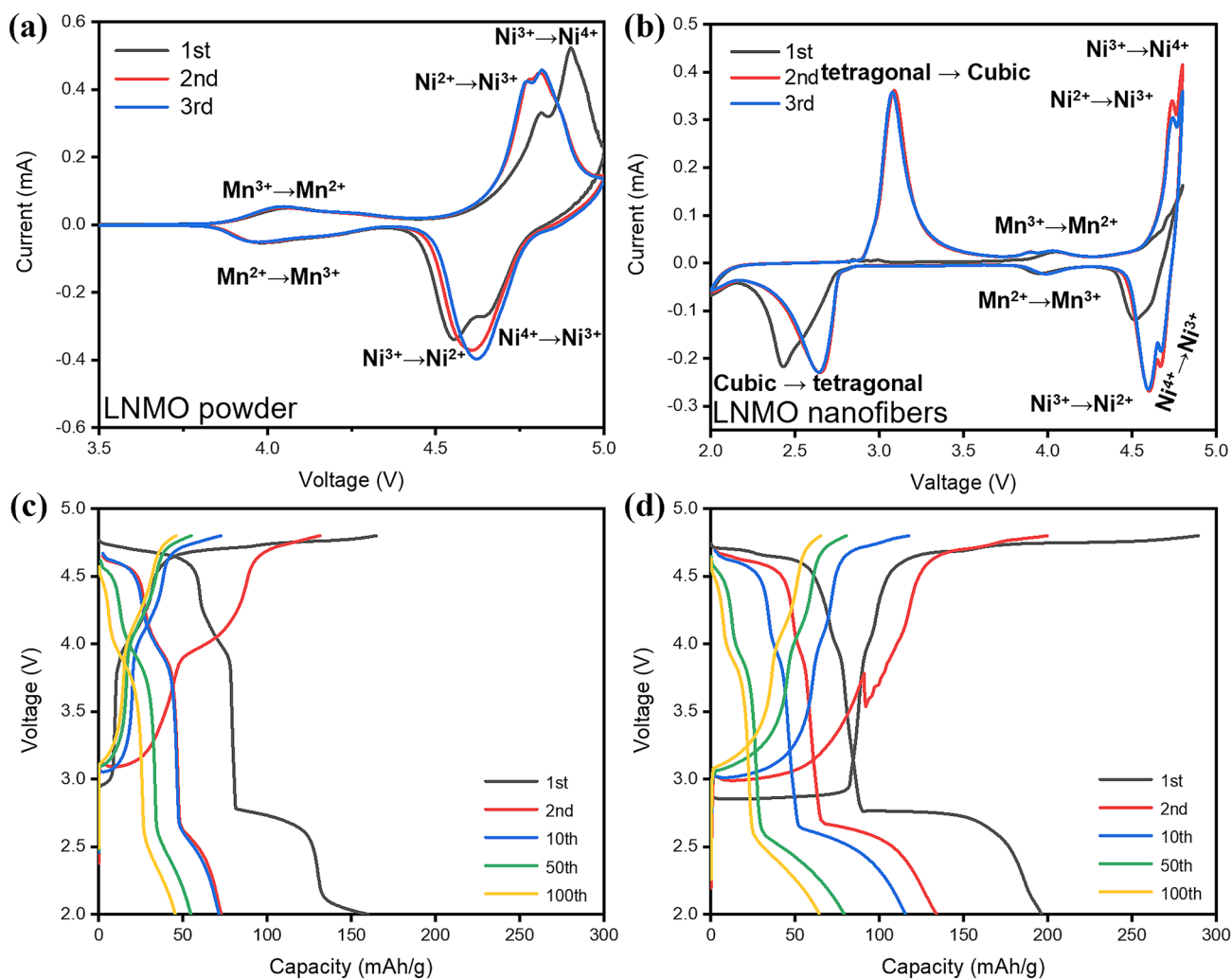

Fig. 4 **a** CV graph of LNMO powder, **b** CV graph of LNMO nanofibers, **c** voltage profile of LNMO powder, **d** voltage profile of LNMO nanofibers

During the initial discharging cycle, a distinct reduction peak was observed at 2.34 V for the LNMO nanofibers, attributed to a phase change from cubic spinel ($Fd3m$) to tetragonal spinel ($I4_1/amd$) [29–31]. After the first cycle, oxidation peaks at 3.08 V appeared for the LNMO nanofibers, indicating a reversible phase transition from tetragonal to cubic phases in the second and third cycles. The cutoff voltage of the LNMO powders was limited up to 3.5 V, as the LNMO bulk particles cannot withstand the strains caused by the phase transformation. Therefore, the voltage plateau associated with the phase variation in the CV data of LNMO powders was not observed. The subsequent oxidation peaks corresponding to the reactions of Ni^{2+}/Ni^{3+} and Ni^{3+}/Ni^{4+} were highly reversible for the control group.

Figure 4c and d displays the charge and discharge voltage curves of the samples. The LNMO nanofibers exhibit several voltage plateaus due to the two-phase reactions, as mentioned in the CV results above. In the 1st, 2nd, 10th, 50th, and 100th cycles, the discharge capacities of the LNMO nanofibers were 196, 134, 115, 79, and 64 mAh/g, respectively. In contrast, the LNMO powder exhibited lower discharge capacities of 160, 73, 71, 55, and 46 mAh/g, respectively, than the LNMO nanofiber. As can be seen in Fig. 4c and d, the nominal voltage for both the LNMO powder and nanofiber is in a similar region. However, the difference between the capacities of LNMO (~ 150 mAh/g) and the nanofiber (~ 200 mAh/g) at the similar nominal voltage region in the first cycle is remarkably higher. A similar kind of capacity difference can be seen in the second and third cycles between LNMO powder and the nanofiber. The capacity difference in the first cycle of LNMO and the nanofiber suggests an approximately 25% higher energy density in the LNMO nanofiber. The voltage characteristics of both LNMO samples appear highly reversible, indicating that the redox reactions for lithiation/delithiation during cycling are based on the same electrochemical behaviors in similar crystal structures. Despite the harsh environment that facilitated (tetragonal ↔ cubic) phase changes for the LNMO nanofibers during reaction with Li^+, it is noticeable that the LNMO nanofibers have a much more stable nanostructure compared to the LNMO powders.

Figure 5 shows a comparison of the electrochemical performance of the LNMO nanofiber/CNT electrode and the LNMO powder electrode over 100 cycles. The formation cycle was conducted at a rate of 0.1C (1C = 140 mA/g), while the charge and discharge cycles for the subsequent 100 cycles were at 1C. The LNMO nanofiber/CNT electrode exhibited a low coulombic efficiency of approximately 68% in both the formation and second cycles. The initial cycle had a specific charge capacity of 289 mAh/g and a discharge capacity of 196 mAh/g. Meanwhile, the second cycle had a specific charge capacity of 200 mAh/g and a specific discharge capacity of 134 mAh/g, indicating a decrease in discharge capacity of 62 mAh/g in the second cycle compared to the formation cycle. The LNMO powder electrode exhibited a charging capacity of 165 mAh/g and a discharging capacity of 160 mAh/g. However, during the second cycle, the charging and discharging capacities decreased to 131 and 73 mAh/g, respectively.

Fig. 5 Comparison of cycle test of LNMO nanofibers/CNT and LNMO powder
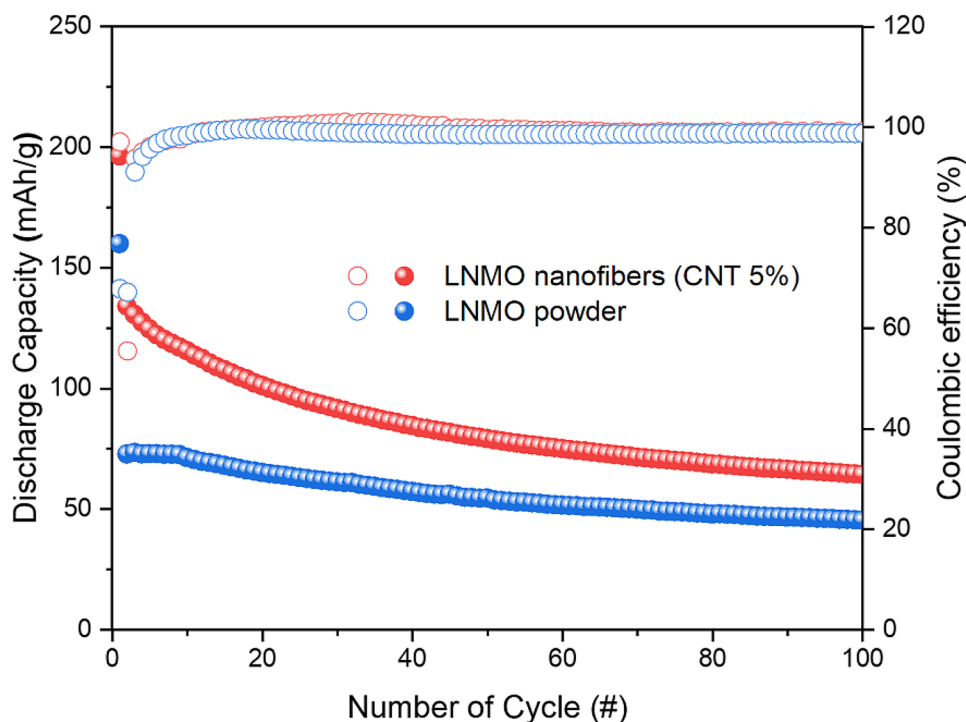
During the formation cycle, the coulombic efficiency was observed to be high at 97%; however, in the second cycle, it significantly decreased to a value of 55%. LNMO nanofibers exhibited a very large initial irreversible capacity due to electrolyte decomposition and manganese elution at high voltages. The reason for the larger irreversible capacity of nanofibers structures lies in their significantly increased surface area compared to bulk LNMO structures, which facilitates the formation of a substantial solid electrolyte interface (SEI) at the interface between the solid electrolyte and the nanofibers. Additionally, LNMO nanofibers electrodes with higher porosity are more likely to absorb liquid electrolyte more readily than LNMO powder electrodes, thereby enabling faster interfacial reactions and the subsequent formation of the SEI [32]. However, over the course of 100 cycles, the LNMO nanofiber electrode with carbon nanotubes as the conductive material demonstrated a higher capacity than the LNMO powder electrode. With a capacity of 66.44 mAh/g, it had a higher capacity than the LNMO powder electrode, which had a capacity of 45.5 mAh/g.

Conclusion

In conclusion, the use of spinel-structured LiNi$_{0.5}$Mn$_{1.5}$O$_4$ (LNMO) as a cathode material for lithium-ion batteries offers economic and eco-friendly advantages. However, low electronic conductivity and volume changes due to phase transitions during charging and discharging at 3 V or lower remain a challenge, resulting in capacity degradation. To address this, LNMO nanofibers were synthesized using the electrospinning method to mitigate volume expansion issues and maintain the structural integrity of the material. Moreover, the electrode was constructed with carbon nanotubes as a conductive material to improve electronic conductivity. Electrochemical evaluations demonstrated that LNMO nanofibers combined with carbon nanotubes exhibited higher capacity and outstanding cyclability compared to LNMO powder, providing a potential solution to the issues faced by conventional LNMO cathodes.

Data Availability The data cannot be made publicly available upon publication because they are not available in a format that is sufficiently accessible or reusable by other researchers. The data that support the findings of this study are available upon reasonable request from the authors.

Declarations

Conflict of Interest The authors have no relevant financial or non-financial interests to disclose.

References

1. M. Winter, B. Barnett, K. Xu, Chem. Rev. **118**, 11433 (2018)
2. K. Duan, J. Ning, L. Zhou, S. Wang, Q. Wang, J. Liu, Z. Guo, A.C.S. Appl, Mater. Interfaces. **14**, 10447 (2022)
3. Q. Liu, X. Su, D. Lei, Y. Qin, J. Wen, F. Guo, Y.A. Wu, Y. Rong, R. Kou, X. Xiao, F. Aguesse, J. Bareño, Y. Ren, W. Lu, Y. Li, Nat. Energy **3**, 936 (2018)
4. J. Liu, Z. Bao, Y. Cui, E.J. Dufek, J.B. Goodenough, P. Khalifah, Q. Li, B.Y. Liaw, P. Liu, A. Manthiram, Y.S. Meng, V.R. Subramanian, M.F. Toney, V.V. Viswanathan, M.S. Whittingham, J. Xiao, W. Xu, J. Yang, X.Q. Yang, J.G. Zhang, Nat. Energy **4**, 180 (2019)
5. C. Wu, J. Lou, J. Zhang, Z. Chen, A. Kakar, B. Emley, Q. Ai, H. Guo, Y. Liang, J. Lou, Y. Yao, Z. Fan, Nano Energy **87**, 106081 (2021)
6. R. Marom, S.F. Amalraj, N. Leifer, D. Jacob, D. Aurbach, J. Mater. Chem. **21**, 9938 (2011)
7. W. Li, E.M. Erickson, Nat. Energy **5**, 26 (2020)
8. T.F. Yi, J. Mei, Y.R. Zhu, J. Power. Sources **316**, 85 (2016)
9. T. Yang, H. Zeng, W. Wang, X. Zhao, W. Fan, C. Wang, X. Zuo, R. Zeng, J. Nan, J. Mater. Chem. A **7**, 8292 (2019)
10. A. Manthiram, K. Chemelewski, E.S. Lee, Energy Environ. Sci. **7**, 1339 (2014)
11. J. Ma, P. Hu, G. Cui, L. Chen, Chem. Mater. **28**, 3578 (2016)
12. R. Xu, X. Zhang, R. Chamoun, J. Shui, J.C.M. Li, J. Lu, K. Amine, Nano Energy **15**, 616 (2015)
13. F. Kong, G. Zhang, D. Wu, F. Sun, S. Tao, S. Chu, B. Qian, W. Chu, L. Song, Chem. Eng. J. **451**, 138708 (2023)
14. E. Lee, K.A. Persson, Nanotechnology **24**, 424007 (2013)
15. Y. Cai, S.Z. Huang, F.S. She, J. Liu, R.L. Zhang, Z.H. Huang, F.Y. Wang, H.E. Wang, RSC Adv. **6**, 2785 (2016)
16. S. Tao, F. Kong, C. Wu, X. Su, T. Xiang, S. Chen, H. Hou, L. Zhang, Y. Fang, Z. Wang, W. Chu, B. Qian, L. Song, J. Alloys Compd. **705**, 413 (2017)
17. H. Zhao, F. Li, X. Shu, J. Liu, T. Wu, Z. Wang, Y. Li, J. Su, Ceram. Int. **44**, 20575 (2018)
18. X. Ding, D. Luo, J. Cui, H. Xie, Q. Ren, Z. Lin, Angew. Chemie - Int. Ed. **59**, 7778 (2020)
19. H. Wu, K. Wang, Y. Meng, K. Lu, Z. Wei, J. Mater. Chem. A. **1**, 6366 (2013)
20. X. Cui, L. Zhang, Y. Hu, D. Yang, J. Zou, J. Alloys Compd. **914**, 165354 (2022)
21. J.G. Wang, H. Liu, H. Liu, X. Li, D. Nan, F. Kang, J. Alloys Compd. **729**, 354 (2017)
22. G. Alva, C. Kim, T. Yi, J.B. Cook, L. Xu, G.M. Nolis, J. Cabana, H.S. Kim, J. Phys. Chem. C **118**, 10596 (2014)
23. Y.-K. Sun, S.W. Oh, C.S. Yoon, H.J. Bang, J. Prakash, J. Power. Sources **161**, 19–26 (2006)
24. N.S. Hansen, D. Cho, Y.L. Joo, Small **8**, 1510 (2012)
25. B. Zhang, Z. Leng, Y. Ling, H. Bai, S. Li, J. Zhou, S. Wang, Crystals **12**, 1624 (2022)
26. J. Song, X. Han, K.J. Gaskell, K. Xu, S.B. Lee, L. Hu, J. Nanoparticle Res. **16**, 2745 (2014)
27. H.A. Tariq, J.J. Abraham, A.A. Quddus, S. AlQaradawi, R. Kahraman, R.A. Shakoor, J. Mater. Res. Technol. **14**, 1377 (2021)
28. J. Liu, J. Wang, Y. Ni, Y. Zhang, J. Luo, F. Cheng, J. Chen, Small Methods **3**, 1900350 (2019)

29. H. Liu, J. Wang, X. Zhang, D. Zhou, X. Qi, B. Qiu, J. Fang, R. Kloepsch, G. Schumacher, Z. Liu, J. Li, A.C.S. Appl, Mater. Interfaces **8**, 4661 (2016)
30. E.S. Lee, A. Manthiram, Chem. Mater. **1**, 3118 (2013)
31. K. Ariyoshi, Y. Iwakoshi, N. Nakayama, T. Ohzuku, J. Electrochem. Soc. **151**, A296 (2004)
32. J.W. Jung, C.L. Lee, S. Yu, I.D. Kim, J. Mater. Chem. A. **4**, 703 (2016)